ACS APPLIED MATERIALS & INTERFACES

Research Article

www.acsami.org

Effect of Thermal Interface on Heat Flow in Carbon Nanofiber Composites

F. Gardea, M. Naraghi,* and D. Lagoudas

Department of Aerospace Engineering, Texas A&M University, 3409 TAMU College Station, Texas 77843-3409, United States

ABSTRACT: The thermal transport process in carbon nanofiber (CNF)/epoxy composites is addressed through combined micromechanics and finite element modeling, guided by experiments. The heat exchange between CNF constituents and matrix is studied by explicitly accounting for interface thermal resistance between the CNFs and the epoxy matrix. The effects of nanofiber orientation and discontinuity on heat flow and thermal conductivity of nanocomposites are investigated through simulation of the laser flash experiment technique and Fourier's model of heat conduction. Our results indicate that when continuous CNFs are misoriented with respect to the average temperature gradient, the presence of interfacial resistance does not affect the thermal conductivity of the nanocomposites, as most of the heat flow will be through CNFs; however, interface thermal resistance can significantly alter the patterns of heat flow within the nanocomposite. It was found that very high interface resistance leads to heat entrapment at the interface near to the heat source, which can promote interface thermal degradation. The magnitude of heat entrapment, quantified via the peak transient temperature rise at the interface, in the case of high thermal resistance interfaces becomes an order of magnitude more intense as compared to the case of low thermal resistance interfaces. Moreover, high interface thermal resistance in the case of discontinuous fibers leads to a nearly complete thermal isolation of the fibers from the matrix, which will marginalize the contribution of the CNF thermal conductivity to the heat transfer in the composite.

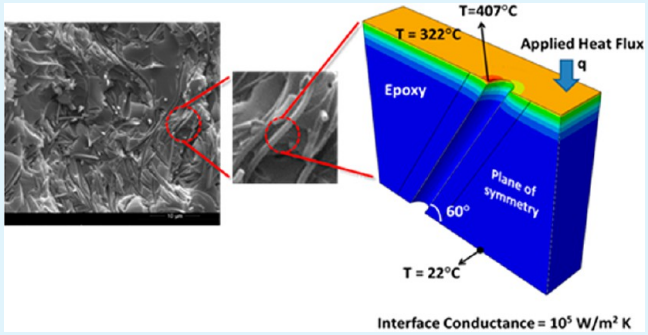

KEYWORDS: *carbon nanofiber composites, thermal interface, heat transfer, thermal degradation*

1. INTRODUCTION

With the advent of nanometer sized electronic devices, such as nanoscale transistors, a challenge in the design and operation of state-of-the-art devices is the presence of "hot spots" where heat flux can exceed ~5 MW/m^2.[1] One way of addressing this heating problem is to incorporate high thermal conductivity materials into the devices and thus dissipate such large fluxes. In addition to micro- or nanoelectronics applications, nanofibers have been shown to reinforce the interface of advanced carbon fiber laminated composites,[2] which have traditionally been used as structural components in aerospace applications. However, even though the main function of these composites is structural, they can be exposed to large temperature fluctuations, such as when subjected to lightning strikes. It has been reported that the nature of lightning strikes consists of multiple high current (up to 80 kA)[3] short pulses (~0.25−200 ms),[3,4] which can generate large heat fluxes in the composite. Addressing fiber composite behavior when subjected to a short heat pulse of large magnitude is of significant importance due to the possibility of thermal degradation within the composite.[5,6] Therefore, developing thermally conductive nanocomposite materials to be used for heat dissipation and structural protection is of significant value. For such applications, polymers offer several advantages, such as processability and relative lightweight. However, polymers typically suffer from low thermal conductivity, which limits their use in high-power density regions, where heat dissipation functionality is of vital importance. To overcome this limitation, incorporation of nanoscale particles with high thermal conductivity, such as carbon nanotubes (CNT) and carbon nanofibers (CNF), into polymers is considered a promising approach to develop nanocomposites with a significantly improved thermal conductivity compared to the neat polymer.[7−9] This approach is inspired by the remarkable thermal conductivity of graphitic nanoparticles, such as CNTs, graphite particles, and vapor grown CNFs, which is in the range of 20−2000 W/(m K),[10−13] significantly larger than the thermal conductivity of typical polymers in the order of 0.1−0.4 W/(m K).[10]

Despite the promising thermal conductivity of such nanoparticles, various studies on thermal properties of graphitic particle−polymer composites show a large scatter, and in most cases only marginal improvements in the thermal conductivity of the nanocomposite upon the addition of nanoparticles to the matrix is observed (Figure 1).[11−19] More interestingly, some studies have suggested that the addition of thermally

Received: October 18, 2013
Accepted: December 17, 2013
Published: December 17, 2013

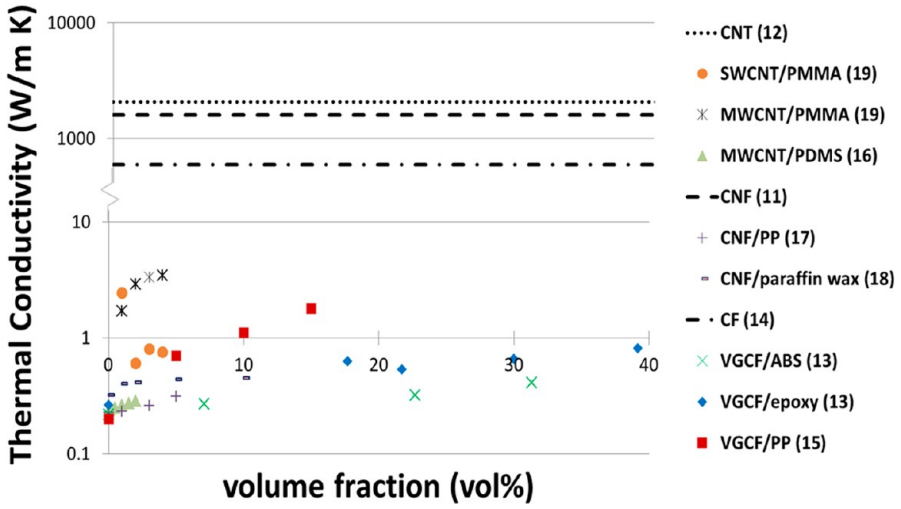

Figure 1. Reported experimental data for thermal conductivity of carbon nanotube (CNT), carbon nanofiber (CNF), and carbon fiber (CF) composites.

conductive particles may even lower the thermal conductivity of the nanocomposite to below the thermal conductivity of the matrix.[20,21]

For example, Yang et al. observed no detectable change in the thermal conductivity of vapor grown carbon nanofiber (VGCNF) liquid crystal polymer composites with VGCNF content of as high as 15 wt %, which was attributed to the nonuniform dispersion of nanofibers and the lack of a percolated network between them.[22] On the other hand, Patton et al. observed a 300% increase in the thermal conductivity of vapor grown carbon fiber (VGCF) polymer composites with 39 vol % VGCF. However, the magnitude of the thermal conductivity remained relatively low (~0.8 W/(m K)) as compared to the intrinsic thermal conductivity of the filler. The low magnitude of composite thermal conductivity was attributed to the low efficiency in transfer of thermal energy between nanofibers.[13]

Several factors may contribute to the scatter in the thermal conductivities of nanocomposites, such as variations in the geometry of individual reinforcements of any type (e.g., CNTs or CNFs) between different experiments and differences in the surface conditions of the nanoscale reinforcement and reinforcement−matrix couplings. For example, Seidel and Lagoudas used a micromechanics approach to model heat transfer in CNT nanocomposites. The results showed that the geometry of the tubes (i.e., the hollowness of the CNT) has a significant effect on the composite thermal conductivity.[23] In addition to geometry, another parameter that contributes to the differences in reported data is the interface coupling between the reinforcement and the matrix.

As the particle size approaches smaller length scales, the interface between particle and matrix will play a more critical role in controlling the heat transfer in the composite, primarily due to the higher surface-to-volume ratio.[24] At the nanoscale, thermal transport becomes especially important when the particle size becomes comparable to the phonon mean free path, which can be in the range of 1−100 nm.[25] This can result in either diffusive, having many scattering events, or ballistic thermal transport of phonons.[26] Every et al. found that the thermal conductivity of ZnS/Diamond composites was dependent on the particle size with the effective composite conductivity decreasing with a decrease in particle size (for submicrometer size particles). The reason for the decrease in thermal conductivity was attributed to the increasing dominance of the interfacial thermal resistance as particle size decreased,[24] which results in significant scattering of phonons.

Heat conduction in carbon materials is dominated by phonons resulting from strong sp^2 covalent bonds,[26] making carbon materials very efficient in the transfer of heat. Weak coupling of phonons, due to the difference in phonon vibration frequencies between the two phases of a nanocomposite (e.g., CNT and the polymer matrix), suppresses the transmission of vibrational modes and heat energy at the interface.[27] This interfacial resistance acts as a boundary layer resistance to heat flow, which leads to a discontinuity of temperature at the interface for any finite heat flux across it.[28] This issue was addressed via molecular dynamics simulations by Shenogin et al., who demonstrated that the heat flow between a CNT and an octane liquid is limited by low frequency phonon vibration modes due to weak coupling at the interface.[29] Through micromechanics modeling of heat transfer in a CNT reinforced nanocomposite and comparison with experimental results, Seidel and Lagoudas showed that the functionalization of the CNT surface can lead to a decrease in the interface thermal resistance,[23] potentially through enhanced mechanical coupling between the surface functional groups of the CNT and the matrix. Gardea and Lagoudas found that even though functionalization of CNTs can lead to a reduction in interfacial thermal resistance between a CNT and an epoxy matrix, the intrinsic thermal conductivity of the CNTs can be significantly reduced,[30] which can be attributed to more scattering sites for phonons in CNTs as a result of the defects and asymmetry created by functionalization.

Even though a full theoretical quantification of the interface thermal resistance requires the consideration of quantized density of states of phonons, continuum heat transfer equations (Fourier's law and conservation of energy) can reliably describe the heat flow in the presence of interface resistance in nanocomposites, by modeling the interface conductivity as a known ratio of heat flux through an interface, for a given temperature jump across that interface.[31] One of the first models to incorporate interface thermal effects was the one presented by Hasselman and Johnson,[32] which suggests that the overall thermal conductivity of the composite may be lower

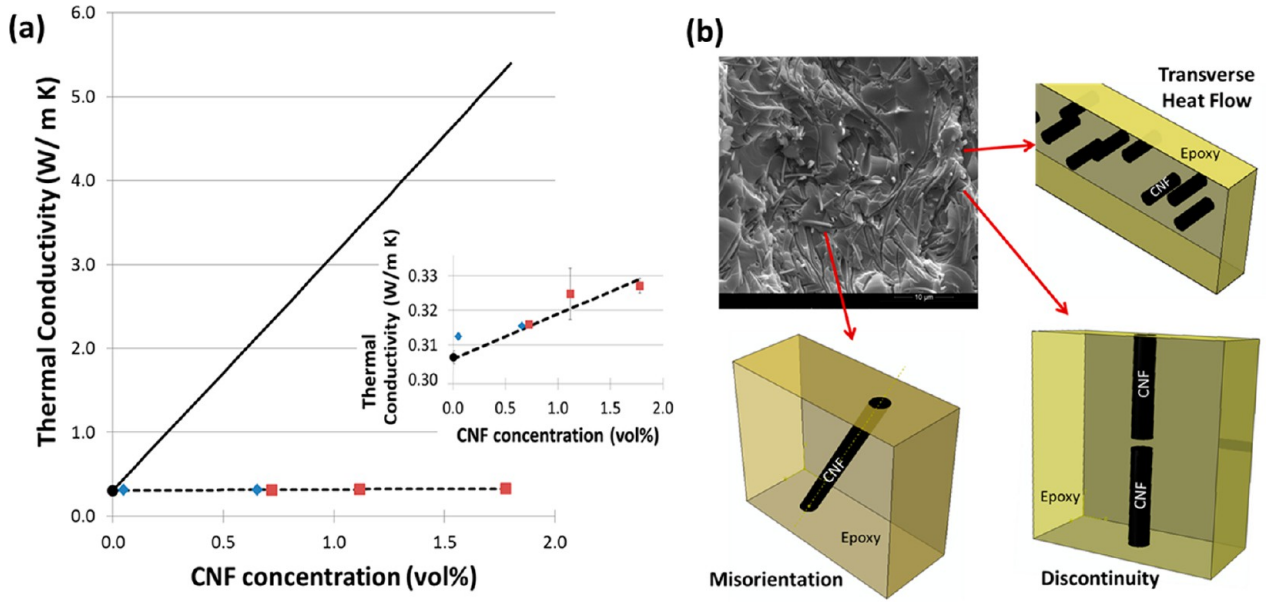

Figure 2. (a) Experimental results for thermal conductivity of CNF/epoxy composites and comparison to micromechanics model with (broken line) and without (solid line) interfacial effects. Inset shows a magnified plot. (b) SEM image of CNF composite cross-section and modeling case studies of CNF discontinuity, orientation, and lateral arrangements.

than that of the matrix when the interfacial conductance is very low, even when the thermal conductivity of the filler is significantly higher than the matrix. Hatta and Taya[33] developed an analytical model based on the equivalent inclusion method to determine the thermal conductivity and temperature profile of coated-fiber composites, where the ratio of thermal conductivity of the fiber to matrix was chosen to be 20 and 1000. Their results show that the thermal properties of the coating (whether highly conductive or resistive) can lead to significant enhancement in the effective composite thermal conductivity or resistivity. Nan et al.[34] introduced a Kapitza interface thermal resistance by considering this thermal resistance as the limiting case of heat transport across phases which are separated by a thin interphase region with poor conduction. Comparison to experimental results showed good agreement for diamond reinforced ZnS and SiC reinforced aluminum. Song and Youn[35] studied the thermal conductivity of carbon nanotube composites via an asymptotic expansion homogenization method and found that the effective thermal conductivity predicted by the asymptotic homogenization method agrees with experimental results, even though no direct interaction between CNTs was considered.

In this paper, we have utilized finite element analysis of heat flow in nanocomposites to investigate potential sources of the scattered thermal conductivities measured in nanocomposites of highly conductive nanoscale reinforcements in a relatively nonconductive matrix. Our study considers the effect of reinforcement discontinuity, alignment, and interface thermal conductance on the heat flow patterns within a composite and on the effective thermal conductivity of the composite. The geometrical parameters of our models are selected to represent our manufactured CNF composites. We have included the interface thermal conductance in our study as a phenomenological parameter that takes into account both the interface thermal resistance between perfectly bonded surfaces and the effect of imperfect fiber−matrix contact, for example, due to lack of wettability of the reinforcements. The former is a result of acoustic impedance mismatch and dissimilarities between the modes of phonon vibration between the two sides of the interface. In addition, the thermal properties of the reinforcements and their dimensions are selected to match the properties of CNFs and a typical epoxy matrix, such as EPON. Despite this specificity, many of the findings of the study, such as the interface thermal degradation, can be applied to the design of other composite materials with thermally conductive fillers and nonconductive matrix. Our results point to the significance of interface thermal resistance not just as a parameter to control thermal conductivity of the nanocomposites but also, and perhaps more importantly, as a means to subside thermal degradation of interfaces in structural nanocomposites that experience sudden temperature changes during their operation.

2. THERMAL CONDUCTIVITY OF CNF COMPOSITES

As a prelude and guide to our computational study of the interface thermal resistance in nanocomposites, we have experimentally explored the thermal conductivity of nanocomposites with random distribution of CNF and with a CNF percolated network, as shown in Figure 2. Carbon nanofibers were fabricated by thermal stabilization and carbonization of polyacrylonitrile (PAN)[36] fibers, which were collected using a rotating drum technique. The PAN nanofibers were electrospun from a 9 wt % solution of PAN in dimethylformamide using an electrospinning distance of ∼20 cm and an electrospinning voltage of ∼15 kV. The PAN nanofibers were then thermally stabilized in air at a temperature of ∼250 °C for ∼3 h followed by carbonization in an inert atmosphere, ultra high purity nitrogen, at ∼1100 °C for another ∼3 h. This method yields CNFs with diameters in the range of ∼200−350 nm.[37] The randomly oriented CNF/epoxy composites were fabricated via solution mixing. For this purpose, the electrospun CNFs were first dispersed in ethanol via ultrasonication for 1 h. Next, EPON 862 epoxy was added to the solution and high shear mixed at 8000 rpm for 1 h. An average length for the CNFs (∼50−200 μm) was obtained. The epoxy−ethanol−CNF solution was then magnetically stirred on a hot plate at a

temperature of 60 °C, under vacuum, until all the solvent evaporated. To prevent the agglomeration of the CNFs, the solution was precured by adding 20% of the required curing agent (EPIKURE W) while continuing to magnetically stir at 120 °C for 200 min, resulting in an increase in the viscosity of the solution. Next, the remaining amount of the required curing agent was added and the solution was fully cured for 8 h at 40 °C followed by 2 h at 120 °C and another 2 h at 175 °C. To achieve weight fractions higher than 1 wt %, a different fabrication method was used consisting of a compact sheet of networked CNFs. The CNFs were first high shear mixed in ethanol and then vacuum filtered to form a freestanding, compact sheet of CNFs. EPON 862 epoxy was then mixed with the appropriate amount of EPIKURE W curing agent using a magnetic stirrer at 60 °C. The epoxy was then degassed in a vacuum oven at 100 °C to remove any air bubbles present. Once all of the air bubbles were removed, the epoxy was poured into a preheated (60 °C) mold. The CNF network compact sheet was then completely submerged in the epoxy. The curing cycle was set to 2 h at 120 °C followed by 2 h at 175 °C.

The thermal conductivity of the CNF nanocomposite samples was determined at room temperature (25 °C) using a Hot Disk thermal constants analyzer. The testing equipment utilizes a resistor with a double spiral disk shape that serves as both a temperature sensor and heat source. The variation in electrical resistance caused by the transient change in temperature is related to the heat flow between the sensor and the specimen, from which the sample thermal conductivity is obtained.[38,39]

The experimental results obtained show a marginal increase in thermal conductivity of about 6.8% over neat epoxy for 2.7 wt % CNF (Figure 2a). In the figure, we have also presented the predictions of the thermal conductivity of an "ideal" nanocomposite of CNFs, where the thermal resistance at the interface of CNFs and the matrix is negligible. The predictions of the thermal conductivity are based on the micromechanics model of heat transfer in nanocomposites developed by Seidel and Lagoudas,[23] which accounts for heat exchanges between nanofibers and the matrix for randomly oriented fibers, with zero interface resistance. Here we have assumed a matrix thermal conductivity of 0.306 W/(m K) and a CNF thermal conductivity of 1000 W/(m K), in the range of the values reported for carbon fibers and nanofibers.[11,14] The aspect ratio was set to 300, similar to what was observed in microscopy images of the fabricated composites (~100 μm average length and 330 nm diameter).

For the predictions of the "ideal" model (solid line in Figure 2b with zero interface thermal resistance) to match the experimentally measured thermal conductivities, the thermal conductivity of the CNFs should be about 330 times lower than the value of the CNF thermal conductivity chosen for this study (1000 W/(m K)) and up to 650 times lower than the values reported for the thermal conductivity of CNFs.[11,17] Alternatively, the discrepancies between the model predictions and experiments can be accounted for by the inclusion of an interphase with finite thermal conductivity between the reinforcements and the matrix in the micromechanics model of Seidel and Lagoudas.[23] When the third phase (interphase) between the fiber and matrix in the micromechanics model is included, with a thickness, t_{int}, of 0.5% of the radius of the CNF, and a thermal conductivity of $k_{int} = 9 \times 10^{-5}$ W/(m K), the model predictions matches the experimental results most accurately. Although physically the concept of interface thermal resistance refers to a temperature jump across an interface with zero thickness,[40] the micromechanics formulation requires the attribution of a finite thickness to the interphase. Hence, in our analysis, the thickness of the interphase is set to a small fraction (0.5%) of the radius of the CNF to minimize circumferential changes in temperature within the interphase. The value for the thermal conductivity of the interphase corresponds to an interface conductance value, h_{int}, of 10^5 W/(m^2 K) through the following relationship $h_{int} = (k_{int}/t_{int})$. This value for the interfacial thermal conductance serves as a motivation and starting point for our study.

The above analysis and the poor comparison between the "ideal" model prediction and the experimental results of thermal conductivities of CNF composites further points to the significance of the factors that affect the heat transfer in the composite material, such as interface thermal resistance and geometrical parameters such as CNF discontinuities. The latter may occur as a result of residual stresses that are developed during the processing of nanocomposites. The CNF discontinuities may also be thought of as CNF−CNF junctions. In the following section, we have addressed the effect of these barriers of heat transfer on the heat flow and thermal conductivity of nanocomposites through finite element analysis.

3. CONTINUUM MODELING OF HEAT TRANSFER IN CNF COMPOSITES

3.1. Problem Definition. To model heat transfer in CNF composites, it is assumed that the medium is composed of two solid materials, CNF and epoxy, as shown in Figure 3. It is assumed that CNFs are straight rods with uniform diameters and identical dimensions, which are homogeneously dispersed in the matrix.

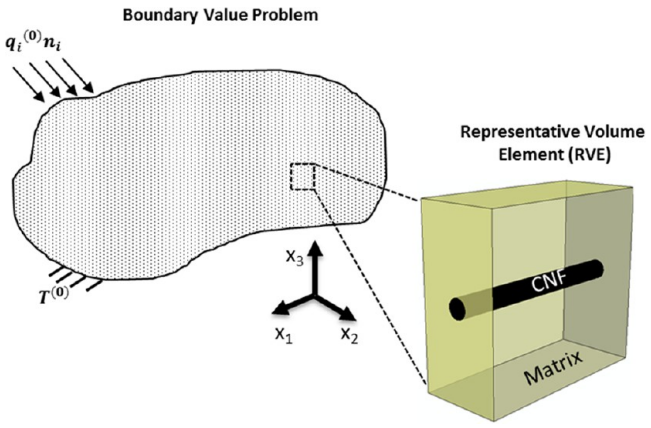

Figure 3. Multiscale schematic of CNF composite showing a CNF embedded in a matrix as a representative volume element (RVE).

For a given set of boundary conditions, such as applied temperature, $T^{(0)}$, and/or applied heat flux, $q_i^{(0)}$, at the macroscale, the steady state heat conduction equation formed the basis for the finite element analysis of the representative volume element (RVE). The heat conduction is mathematically expressed by eqs 1 and 2 for each constituent, where k_{ij}^{m} and k_{ij}^{CNF} are the thermal conductivity of the matrix and CNF, respectively, and T_m and T_{CNF} are the temperature of the matrix and CNF, respectively. It is assumed that the heat flux obeys Fourier's Law of heat conduction.

$$\frac{\partial}{\partial x_i}\left(k_{ij}^{m}\frac{\partial T_m}{\partial x_j}\right)=0 \quad (1)$$

$$\frac{\partial}{\partial x_i}\left(k_{ij}^{CNF}\frac{\partial T_{CNF}}{\partial x_j}\right)=0 \quad (2)$$

Although the micromechanics formulation (Section 2) requires a finite thickness to account for the interface thermal resistance, in this section and for the purposes of finite element analysis, the interface has zero thickness, with a finite temperature discontinuity for a given heat flux through the interface. The ratio of the heat flux to the temperature discontinuity is the interface heat conductivity of the CNF−matrix interface, which is a property of the interface. It is assumed that there is a continuous heat flux, in the outward normal n_i direction, at the CNF−matrix interface (eq 3). When the concept of interface thermal resistance is introduced, the finite temperature discontinuity across the interface is captured by eq 4, where h_{int} is the interfacial thermal conductance.

$$k_{ij}^{CNF}\frac{\partial T_{CNF}}{\partial x_j}n_i=k_{ij}^{m}\frac{\partial T_m}{\partial x_j}n_i \quad (3)$$

$$-k_{ij}^{CNF}\frac{\partial T_{CNF}}{\partial x_j}n_i=h^{int}(T_{CNF}-T_m) \quad (4)$$

Complementary to the above Fourier method approach, the conditions of heat transfer in a laser flash experiment were modeled for the one-dimensional case, to explore the response of the material to thermal shocks. This method was simulated by applying a short pulse of heat to the top surface of the composite and monitoring the temperature rise, as a function of time, on the opposite surface of the material. The rate at which the heat pulse diffuses, thermal diffusivity α, through the composite is obtained through eq 5, where $t_{1/2}$ is the time when the monitored surface reaches half the maximum temperature and t is the thickness of the sample. Therefore, the effective thermal conductivity of the sample, k_{eff}, from the finite element simulated laser flash experiment can be calculated as

$$k_{eff}=c_p\rho\alpha \quad \text{where } \alpha=\frac{1.38t^2}{\pi^2 t_{1/2}} \quad (5)$$

where c_p is the composite heat capacity, and ρ is the composite density.[41] The laser flash method simulates a real-life scenario in which the composite sample is placed near a heat source, at a time when a sudden rise of temperature is experienced.

3.2. Solution Methodology. To shed light on discrepancies between experimental results and modeling predictions, we studied the heat transfer in CNF nanocomposites via finite element analysis (FEA) and used it as an approximation to obtain a numerical solution. Our FEA model was inspired by the structure of a CNF composite. To make a realistic model of CNF composites, the cross-section of CNF composite samples were studied via scanning electron microscopy (SEM), as shown in Figure 2b. Given the significantly higher thermal conductivity of CNFs compared to neat epoxy, we assumed the heat flow is mostly through CNFs. Therefore, the effect of the following parameters on heat transfer within the nanocomposite was studied: volume fraction (studied in the case of lateral thermal conductivity), orientation of CNFs, and CNF discontinuities. The latter parameter also reflects the effect of CNF−CNF junctions on heat transfer. The geometrical correspondence between the model and experiments are shown in Figure 2b. In addition, the model discretely accounts for interface thermal resistance effects. In exploring the effect of CNF discontinuity, we considered the common understanding that according to,[42] even when thermally conductive reinforcements are nearly touching each other in a nonconductive matrix, heat will flow through an interface-like resistance before entering the other tube.

The heat transfer analysis of the composites studied involved the use of the commercial finite element software package, ABAQUS. The effect of CNF orientation was modeled by employing a combination of 3D quadratic heat transfer hexagonal elements (DC3D20) and tetragonal (DC3D10) elements. In all cases, the interface thermal resistance was modeled as a surface thermal resistance (surface-to-surface contact with a finite thermal conductance property) between the CNF and epoxy matrix. Specifically, low volume concentrations were studied as it is typically the case for nanoscale reinforcements. For the CNF orientation studies, the volume fraction was kept constant at 2 vol %, similar to the volume fraction fabricated in experiments.

By exploiting the symmetry of the model in the third dimension, 3D models were reduced to two dimensions to study the effect of interface thermal conductance on the lateral thermal conductivity for various volume fractions. Similarly, 2D models were created to study the effect of fiber discontinuity in a composite with a single CNF (can also be thought of as CNF−CNF junctions). Quadratic heat transfer quadrilateral (DC2D8) elements were used for the mesh. The mesh was refined until the solution was comparable to that obtained from an analytical solution whenever possible, thus verifying convergence. The gap distances, g, studied for the discontinuous CNF cases were $d/10$, $d/2$, d, and $2d$, where d = 330 nm is the diameter of the CNF in the models, which is set to be equal to the experimentally measured average diameter of CNFs. A thermal conductivity value of 1000 W/(m K) was used for the CNF, comparable to values reported in literature.[11] The thermal conductivity of the epoxy matrix, with a value of 0.306 W/(m K), was used and obtained from experimental testing. The heat capacity for the CNF was set to 0.716 J/(g K), assuming it is similar to that of graphite,[43] while the heat capacity of epoxy was set to 1.06 J/(g K).[44] The values used for density were 1.80 and 1.17 g/cm^3 for CNF and epoxy, respectively.[45,46] For the Fourier method, constant temperature boundary conditions were maintained at each surface, with the top surface being kept at 310 °C and the bottom surface at 300 °C.

4. RESULTS AND DISCUSSION

4.1. Thermal Conductivity of Nanocomposites. As the first step to investigate the roots of discrepancies between model and experiments of the heat transfer in CNF−epoxy nanocomposites (Figure 2 a), we have explored the effect of CNF orientation and interface thermal conductance on the overall thermal conductivity of the nanocomposite. The interface thermal conductance values explored in this study range from 10^4 to 10^7 W/(m^2 K), guided by reported experiments and simulations[15,29,47] and also by the value of 10^5 W/(m^2 K) obtained from fitting the micromechanics model to the obtained experimental data.

To this end, we first considered the heat flow in nanocomposites, when the overall temperature gradient is

dx.doi.org/10.1021/am4046102 | ACS Appl. Mater. Interfaces 2014, 6, 1061−1072

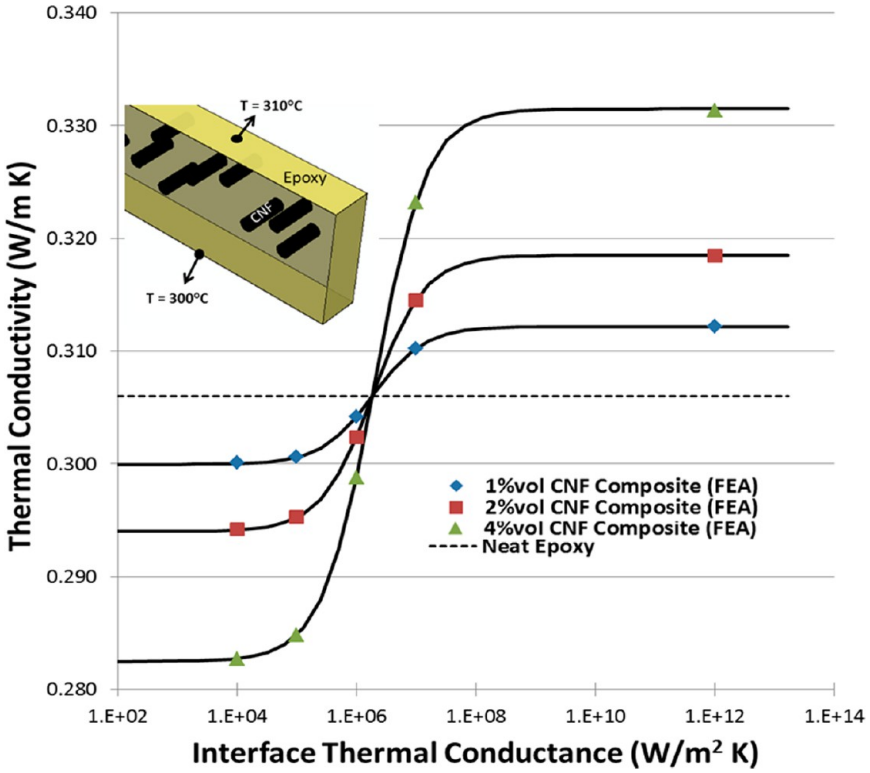

Figure 4. Transverse thermal conductivity as a function of interface thermal conductance for various CNF volume fractions obtained from finite element analysis. Results follow the predictions by Hasselman–Johnson analytical model (solid lines).

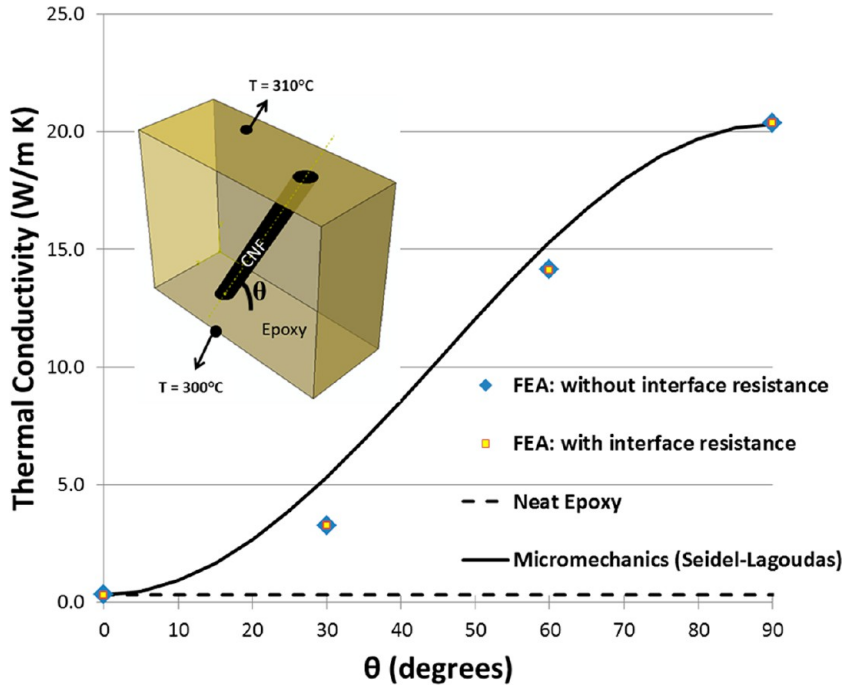

Figure 5. Thermal conductivity as a function of CNF orientation angle (θ) with and without accounting for interfacial effects. Interface thermal conductance = 10^5 W/(m^2 K).

perpendicular to CNFs (inset of *transverse heat flow* in Figure 2b). The nanocomposite schematic structure and the average thermal conductivity of the nanocomposite, calculated from the Fourier model of heat transfer (Section 3.1), as a function of interface resistance and fiber volume fraction, are presented in Figure 4. For each volume fraction, several cases of randomly distributed nanofibers were studied to capture potential variations of the thermal conductivity with nanofiber distribution. The results show that, with a random distribution of nanofibers in the model, the dependence of the thermal conductivity on nanofiber distribution was negligible (less than 0.22% variations between randomly distributed cases).

dx.doi.org/10.1021/am4046102 | ACS Appl. Mater. Interfaces 2014, 6, 1061–1072

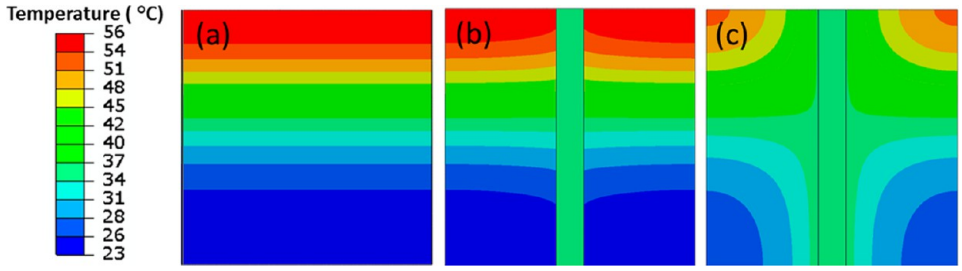

Figure 6. Steady state thermal contours for (a) neat epoxy, (b) CNF at 90° finite interface conductance (interface thermal conductance = 10^5 W/(m^2 K)), and (c) infinite interface conductance. (CNF is vertical and is in the middle of (b) and (c)).

In addition, this analysis indicates that the potential negative/positive contribution of the thermal conductivity of CNFs on the heat transfer in nanocomposites hinges around the interface thermal conductivity between CNFs and the matrix. For instance, with a very high interface thermal conductance (>~10^6 W/(m^2 K)), the thermal conductivity of the nanocomposites will increase by increasing the volume fraction of the CNFs. On the other hand, despite the fact that thermal conductivity of CNFs is more than 3 orders of magnitude higher than the matrix, poor interface conductance (<~10^6 W/(m^2 K)) will thermally isolate CNFs from the matrix. In this case, the overall thermal conductivity of the matrix will decrease by adding more CNFs. Therefore, quantitatively, up to ~4 vol % of CNFs in an epoxy can result in ~10% enhancement (reduction) in the lateral thermal conductivity of the nanocomposite, when the interface thermal resistance is negligible (very high). The results follow the prediction of the Hasselman–Johnson model, which considers the presence of a thermal resistance at the interface.[32]

On the other hand, when fibers are continuous and not perpendicular to the overall temperature gradient, our FEA analysis shows that the heat flow is mainly through the CNF and the thermal conductivity becomes rather independent of the interfacial thermal resistance (Figure 5). Our FEA results follow the predictions of the micromechanics model of Seidel and Lagoudas.[23]

4.2. Heat transfer in Composites Reinforced with Inclined CNFs. Although interface thermal resistance between CNFs and the matrix only marginally affects the thermal conductivity of nanocomposites (Figure 5), it highly controls the temperature distribution and heat flow within the matrix. This fact has significant implications in the structural health of nanocomposites which experience sudden changes in temperature during their operation. Figure 6 shows this effect when a CNF is laid parallel to the heat flow.

For very low interface thermal conductance (~10^5 W/(m^2 K) or less[15]), the temperature contours within the matrix are more or less the same as the ones in the neat epoxy (Figure 6a,b). In this case, heat flow through the CNF remains within the CNF boundary and only minimally influences the heat flow in the surrounding matrix. On the other hand, when interface thermal resistance is negligible (Figure 6c), heat is allowed to transfer from the matrix to the CNF and vice versa in an accelerated rate. A consequence of this effect is a temperature *homogenization* in the matrix, which reduces the heat flow within the matrix, due to suppressed temperature gradients. Similar dependencies of heat flow and temperature gradient on interface thermal resistance is observed in other CNF inclination angles studied (labeled as *Misorientation* in Figure 2b). This dependence of heat flow path on interface thermal resistance will promote the development of locally heated spots at the CNF–matrix interface, when the material is experiences thermal shocks. This phenomenon is referred to herein as *interface heat entrapment*, as explained in the following section.

4.3. Interface Heat Entrapment Due to Interface Thermal Resistance. The heat entrapment at the CNF–matrix interface occurs when the nanocomposite is subjected to a sudden heat flux on one of its surfaces (thermal shock), for instance during a laser flash experiment, or equivalently when it is located near a "hot spot" in a nanoelectronic device during a power surge. To model this case in our FEA, a uniform heat pulse with short duration (0.1 ns) is applied to the top surface of the sample, and the heat propagation through the material is simulated (Figure 7). The temperature history is recorded throughout the transient analysis.

The heat entrapment at the interface of the CNFs and the matrix, at sufficiently poor interface thermal conductance, can be realized from the temperature contours of the nanocomposite (Figure 7) after 0.1 μs of the initial heat pulse. For instance, a CNF nanocomposite with a relatively poor interface thermal conductance of 10^5 W/(m^2 K), in which CNFs make an angle of 60° with the average temperature gradient, will experience a localized rise in temperature that is, at its peak, about 1 order of magnitude higher than the local temperature rise of a similar CNF nanocomposite with a higher interface thermal conductance of 10^7 W/(m^2 K) (on the high end of the experimentally measured interface thermal conductance of composite materials[29,47]), as presented in Figure 7b. In other words, at sufficiently low interface thermal conductance values (e.g., 10^5 W/(m^2 K)), the interface will promote heat accumulation at the interface.

Moreover, for such low interface thermal conductance (10^5 W/(m^2 K)), increasing the projected area of CNF on the top surface of the nanocomposite (normal plane to the average temperature gradient), via changing the orientation of the CNF, increases the magnitude of interface heat entrapment, as it introduces more interface areas with suppressed heat transfer on the heat transfer path. This trend becomes evident by comparing the maximum interface temperature in CNF nanocomposites for the thermal conductance value of 10^5 W/(m^2 K) at different CNF orientations (Figure 7a–c).

In contrast, for relatively high interface thermal conductance (e.g., 10^7 W/(m^2 K)), the interface will facilitate the dissipation of heat along the interface and through the CNF. Therefore, for very high interface conductance (10^7 W/(m^2 K)), increasing the projected area of the CNF on the top surface of the nanocomposite lowers the interface maximum transient temperature (Figure 7a–c).

The interface heat entrapment and the localized temperature rise, for low values of interface thermal conductance, will

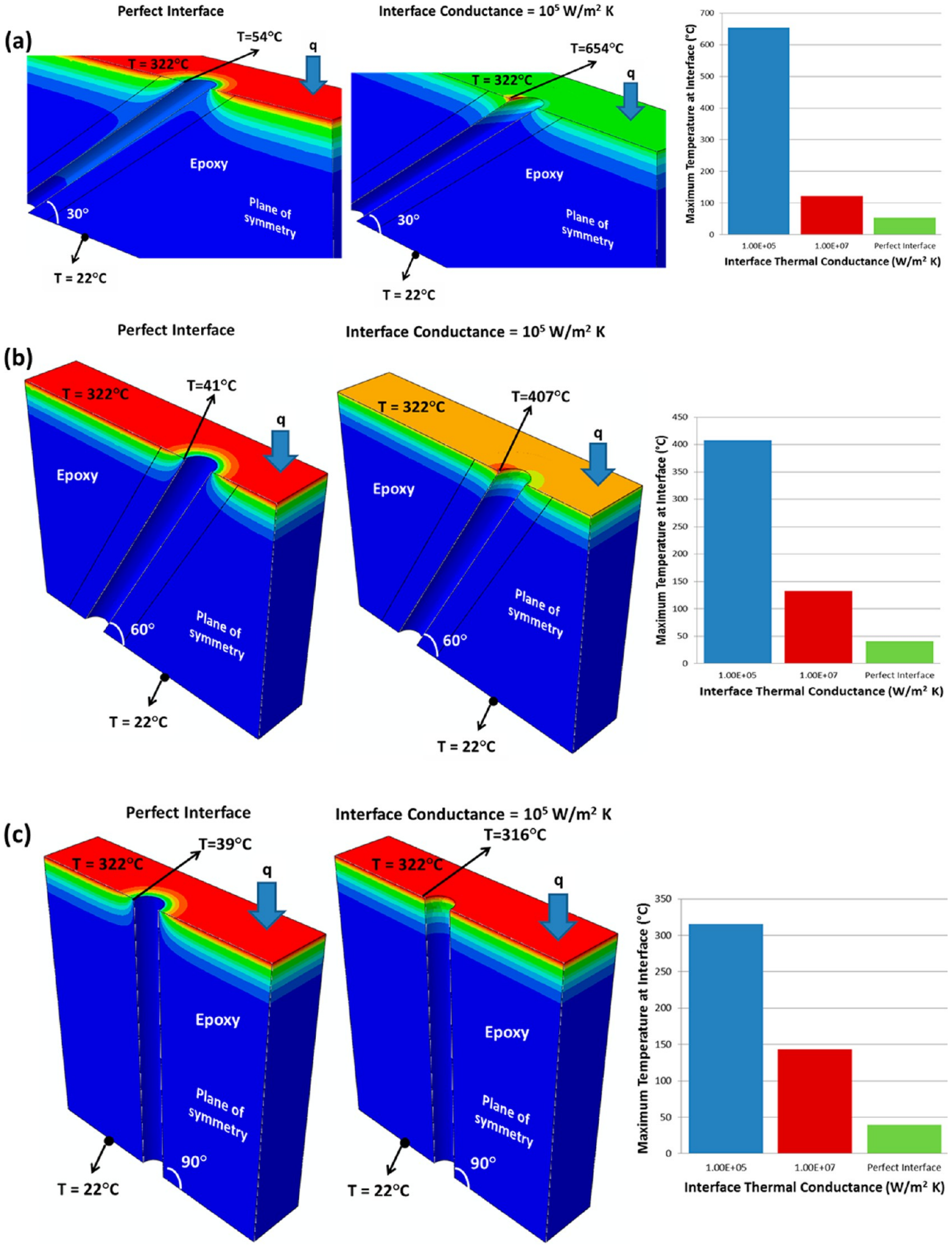

Figure 7. Temperature contour plots for oriented CNFs at 0.1 μs after the heat pulse is applied to the top surface for a CNF inclination angle of (a) 30°, (b) 60°, and (c) 90°. Only matrix is shown; CNF was removed (hollow region) for observation of interface. "Perfect interface" refers to zero interface thermal resistance.

dx.doi.org/10.1021/am4046102 | ACS Appl. Mater. Interfaces 2014, 6, 1061−1072

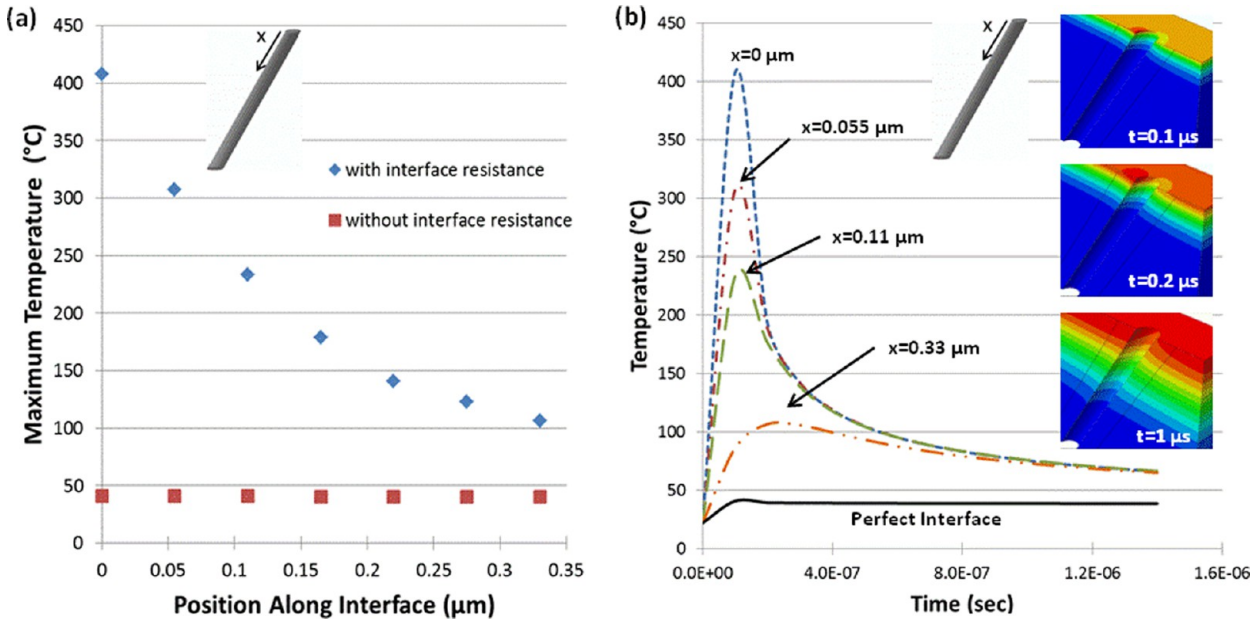

Figure 8. (a) Maximum temperature profile along CNF interface for an inclination angle of 60° after (0.1 μs) the initial heat pulse is applied. (b) Temperature profile along CNF interface for various distances from applied heat pulse as a function of time. Interface thermal conductance = 10^5 W/(m^2 K).

generate a temperature gradient on the CNF−matrix interface that will guide the entrapped heat in the matrix along the interface. As a result, the localized heated interface will not be limited to the top surface of the nanocomposite; rather, the heat will get distributed along the interface, as shown in Figure 8. The distribution of the heat along the interface will reduce the maximum transient temperature. For instance, the redistribution of heat from x = 0 to x = 0.33 μm, reduces the peak temperature from 407 °C to 107 °C.

This local heating of the interface and the propagation of the hot spot along the interface can result in thermal degradation of the polymer near the interface, and it is likely to accelerate fiber−matrix debonding under thermomechanical loads. These results further point to the importance of interface thermal conductance engineering in nanocomposites as a means to postpone interface thermal degradation.

4.4. Heat Transfer in Composites Reinforced with Discontinuous CNFs. Another factor that can significantly alter the heat flow within nanocomposites is the discontinuity of reinforcements (or equivalently, the CNF−CNF junctions), which can occur, for instance, as a result of the residual stresses that develop in the material during processing or curing of the matrix. The effect of fiber discontinuity on heat transfer in nanocomposites is strongly dependent on the interface resistance between CNFs and the matrix. The correlation between heat flow patterns within a nanocomposite, the interface thermal conductivity between CNF and the matrix, and the discontinuities of CNF is presented in Figure 9. This figure shows the steady state heat flow when the temperature difference between the top and bottom surface is set to an arbitrary value of 10 °C.

One of the interesting aspects of steady state heat flow in a nanocomposite with discontinuous nanofibers, when the thermal conductivity of the nanofiber is significantly higher than the matrix, is the temperature distribution in the fiber. A combined effect of the interface resistance at the broken ends of the fiber and the high resistance of the matrix between the disrupted ends of the nanofiber suppresses the heat flow between the two portions of the fiber (or two nanofibers at a CNF−CNF junction). This leads to a redistribution of heat and a reduction in the temperature gradient within the fiber. For instance, the temperature gradient in discontinuous nanofibers with a gap of 2d, with d being the nanofiber diameter, and the interface thermal conductivity of 10^5 W/(m^2 K), is 0.05% of the temperature gradient in a continuous nanofiber, when subjected to the same boundary condition as in Figure 9. Therefore, the heat flux within the CNF will be suppressed by almost the same ratio (0.06%), compared to continuous CNFs subjected to similar boundary conditions. Therefore, the effectiveness of CNFs in heat flow within the nanocomposites will be substantially reduced. This ratio will increase by reducing the spacing between CNFs and the interface thermal resistance. For instance, for a gap of d/10 with no interface resistance, the heat flux will be suppressed to about 3.89% (compared to the previous value of 0.06%, stated above) of the heat flux within the continuous CNF.

The discontinuity in the CNFs will also have a significant effect on the heat flow within the matrix. Regardless of the magnitude of discontinuity (gap between the two halves of CNF), at very low interface thermal conductance, (~10^5 W/(m^2 K)[15]), the presence of the discontinuous CNF will have a negligible effect on the temperature contours in the matrix compared to neat epoxy (Figure 9b,d). In other words, similar to the case of a continuous CNF, which is parallel to the heat flow (Section 4.2), high interface resistance will thermally isolate the CNF from the matrix. On the other hand, when the interface thermal resistance is negligible (Figure 9a,c), the presence of the CNF, with its significantly higher conductivity than the matrix, will have a distinct effect on the temperature distribution and heat flow around CNF. Most notably, the high thermal conductivity CNFs will act as a heat sink/source, to reduce the temperature gradient in the matrix (Figure 9e,f). This effect will suppress the heat conduction within the matrix.

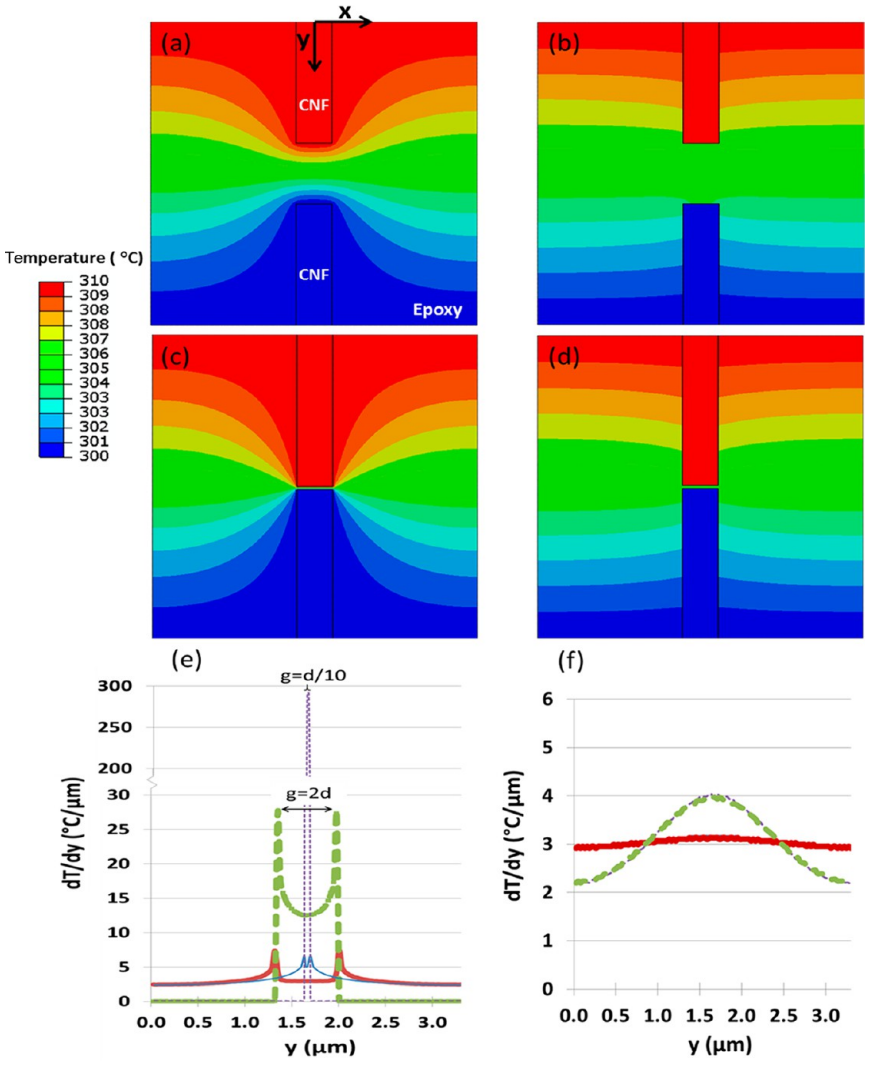

Figure 9. Steady state temperature profile of discontinuous fiber with $g = 2d$ (a) without interface effects and (b) with interface effects (10^5 W/(m^2 K)); $g = d/10$ (c) without interface effects and (d) with interfacial effects (10^5 W/(m^2 K)); (e) gradient of temperature at fiber/matrix interface and (f) gradient of temperature far from fiber principal axis ($2d$ and $d/10$ gap plots overlap). Solid line represents composite with interface resistance whereas broken line represents a perfect interface (zero interface resistance). Thick line represents a gap of $2d$ whereas a thin line represents a gap of $d/10$.

It is worth mentioning the interplay between interface thermal resistance and gap distance in modulating the thermal conductivity of the nanocomposite with discontinuous nanofibers. As the gap spacing between CNFs increases, the temperature gradient in the CNF and heat flux within the CNF will drop. In addition, increasing the interface resistance between CNF and the matrix will suppress the temperature gradient in the CNF and heat flux within the CNF. On the other hand, for very low interface conductance values (~10^5 W/(m^2 K)[15]), the temperature gradient in the matrix will not be affected by the rather uniform temperature distribution in the CNF. Therefore, high interface resistance will increase the heat flux within the matrix.

The competing effect of the gap distance and interface resistance is evident in Figure 10. At relatively large gap distances (about the CNF radius), heat flow within the nanocomposite is predominantly through the matrix. In this case, reducing the interface resistance will facilitate the temperature redistribution (homogenization) in the matrix, via heat exchanges with the CNF, resulting in suppressed heat flux within the matrix and thus reduced conductivity of the nanocomposite. On the other hand, at a relatively low gap distance (~0.20d), heat flow within the nanocomposite is predominantly through the CNF. In this case, reducing the interface resistance will facilitate the heat flow through the CNF, resulting in enhanced conductivity of the nanocomposite.

5. CONCLUSION

This study points to the significance of thermal interface resistance in modulating the heat flow within nanocomposites that are composed of high aspect ratios and thermally conductive reinforcements in a matrix with low thermal conductivity. It was observed that, although the interface thermal conductance only marginally affects the thermal conductivity of nanocomposites with continuous reinforcements, it has a significant effect on the patterns of heat flow and temperature distribution in the material under both steady state and transient conditions. For instance, during a transient response to a heat pulse on one surface, when the interface thermal conductance is very low, the nanocomposite will

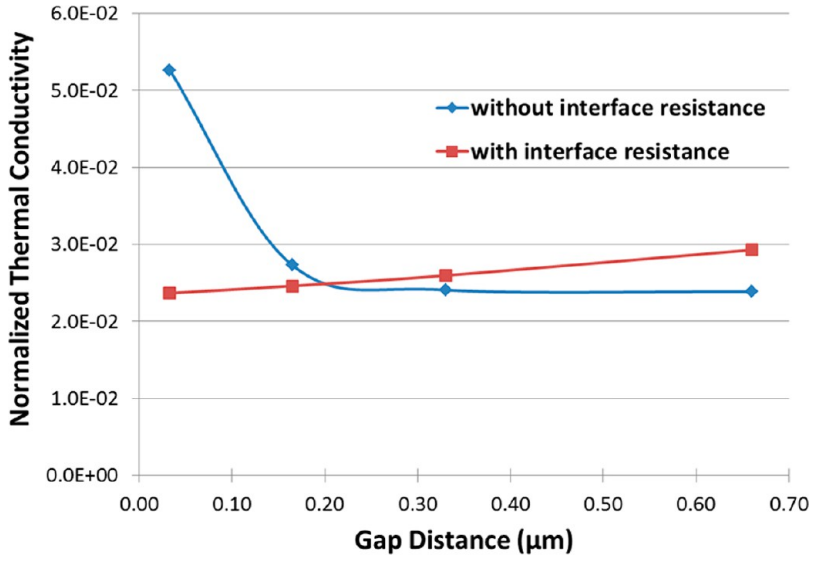

Figure 10. Composite thermal conductivity as a function of gap distance between CNFs. Interface thermal conductance = 10^5 W/(m^2 K).

experience an area of heat concentration at the interface between the CNF and matrix. This interface heat entrapment will generate high temperatures and temperature gradients locally, which leads to the flow of the heated zone along the interface. For poor interface conductivities, the magnitude of the entrapped heat and the elevated temperature increases as the nanofibers projected area in the direction perpendicular to the overall temperature gradient increases. The propagation of this trapped heat through the interface can promote CNF−matrix debonding and can adversely affect the mechanical properties of the nanocomposites.

The discontinuity of nanofibers within the nanocomposite has a drastic effect on both the patterns of heat conduction and thermal conductivity of nanocomposites. In general, at relatively large gaps (a few times the diameter of the CNFs) between the pieces of discontinuous nanofibers or the spacing between neighboring nanofibers, the interface thermal resistance will reduce the temperature gradient and thus heat flux within the nanofibers. On the other hand, very low interface thermal resistance will reduce the heat flux within the matrix by promoting nanofiber−matrix heat exchange. Therefore, at relatively large gap distances, low interface resistance will facilitate the temperature redistribution (homogenization) in the matrix, resulting in reduced heat flow within the nanocomposite. On the other hand, at relatively small gap distance, heat flow within the nanocomposite is predominantly through CNF. Hence, reducing the interface resistance will facilitate the heat flow through CNF, resulting in enhanced conductivity of the nanocomposite.

Therefore, our finite element analysis of the heat transfer in nanocomposites suggests that the effective thermal conductivity of nanocomposites may be reduced by 2−3 orders of magnitude by introducing nanofiber discontinuities or nanofiber−nanofiber junctions on the heat conduction path, whereas other parameters, such as nanofiber misorientation with respect to overall temperature gradient and interface thermal resistance, affect the thermal conductivity of nanocomposite to a lesser degree.

AUTHOR INFORMATION

Corresponding Author

*M. Naraghi. Tel.: (979) 862-3323. Fax: 979-845-6051. E-mail address: Naraghi@aero.tamu.edu. Webpage: http://aero.tamu.edu/faculty/naraghi.

Notes

The authors declare no competing financial interest.

ACKNOWLEDGMENTS

The authors would like to acknowledge the Microscopy Imaging Center (MIC) at Texas A&M University for the use of SEM. The FE-SEM acquisition was supported by the NSF grant DBI-0116835, the VP for Research Office, and the TX Eng. Exp. Station. M.N. would also like to acknowledge the support from Aerospace Engineering department and TAMU through the faculty research funds.

REFERENCES

(1) Balandin, A. A. *Nanotechnol. Mag., IEEE* **2011**, *5*, 15−19.
(2) Dzenis, Y. A. *Science* **2008**, *319*, 419−420.
(3) Krider, E. P.; Uman, M. A. *Wiley Encyclopedia of Electrical and Electronics Engineering*, 1999; pp 350−357.
(4) Larsson, A.; Lalande, P.; Bondiou-Clergerie, A.; Delannoy, A. *J. Phys. D: Appl. Phys.* **2000**, *33*, 1866−1875.
(5) Chippendale, R.; Golosnoy, I. O.; Lewin, P. Numerical modelling of the damage caused by a lightning strike to carbon fibre composites. In *Proceedings of the International Conference on Lightning and Static Electricity*, Oxford, GB, September 6−8, 2011; pp 1−7.
(6) Ramanujam, N.; Vaddadi, P.; Nakamura, T.; Singh, R. P. *Compos. Struct.* **2008**, *85*, 175−187.
(7) Sihn, S.; Ganguli, S.; Roy, A. K.; Qu, L.; Dai, L. *Compos. Sci. Technol.* **2008**, *68*, 658−665.
(8) Hammel, E.; Tang, X.; Trampert, M.; Schmitt, T.; Mauthner, K.; Eder, A.; Pötschke, P. *Carbon* **2004**, *42*, 1153−1158.
(9) Liu, J.; Olorunyomi, M. O.; Lu, X.; Wang, W. X.; Aronsson, T.; Shangguan, D. New nano-thermal interface material for heat removal in electronics packaging. In *Proceedings of the Electronics System Integration Technology Conference*, September 2006; IEEE: 2006; pp 1−6.
(10) Han, Z.; Fina, A. *Prog. Polym. Sci.* **2011**, *36*, 914−944.
(11) Mahanta, N. K.; Abramson, A. R.; Lake, M. L.; Burton, D. J.; Chang, J. C.; Mayer, H. K.; Ravine, J. L. *Carbon* **2010**, *48*, 4457−4465.

(12) Fujii, M.; Zhang, X.; Xie, H.; Ago, H.; Takahashi, K.; Ikuta, T.; Abe, H.; Shimizu, T. *Phys. Rev. Lett.* **2005**, *95*, 1−4.
(13) Patton, R.; Pittman, C., Jr; Wang, L.; Hill, J. *Composites, Part A* **1999**, *30*, 1081−1091.
(14) Zhang, X.; Fujiwara, S.; Fujii, M. *Int. J. Thermophys.* **2000**, *21*, 965−980.
(15) Macedo, F.; Ferreira, J. *Rev. Sci. Instrum.* **2003**, *74*, 828−830.
(16) Hong, J.; Lee, J.; Hong, C. K.; Shim, S. E. *Curr. Appl. Phys.* **2010**, *10*, 359−363.
(17) Sui, G.; Jana, S.; Zhong, W.; Fuqua, M.; Ulven, C. *Acta Mater.* **2008**, *56*, 2381−2388.
(18) Cui, Y.; Liu, C.; Hu, S.; Yu, X. *Sol. Energy Mater. Sol. Cells* **2011**, *95*, 1208−1212.
(19) Hong, W.-T.; Tai, N.-H. *Diamond Relat. Mater.* **2008**, *17*, 1577−1581.
(20) Moisala, A.; Li, Q.; Kinloch, I.; Windle, A. *Compos. Sci. Technol.* **2006**, *66*, 1285−1288.
(21) Gojny, F. H.; Wichmann, M. H.; Fiedler, B.; Kinloch, I. A.; Bauhofer, W.; Windle, A. H.; Schulte, K. *Polymer* **2006**, *47*, 2036−2045.
(22) Yang, S.; Lozano, K.; Lomeli, A.; Foltz, H. D.; Jones, R. *Composites, Part A* **2005**, *36*, 691−697.
(23) Seidel, G. D.; Lagoudas, D. C. *J. Appl. Mech.* **2008**, *75*, 1−9.
(24) Every, A.; Tzou, Y.; Hasselman, D.; Raj, R. *Acta Metall. Mater.* **1992**, *40*, 123−129.
(25) Cahill, D. G.; Ford, W. K.; Goodson, K. E.; Mahan, G. D.; Majumdar, A.; Maris, H. J.; Merlin, R.; Phillpot, S. R. *J. Appl. Phys.* **2003**, *93*, 793−818.
(26) Balandin, A. A. *Nat. Mater.* **2011**, *10*, 569−581.
(27) Hu, M.; Keblinski, P.; Schelling, P. K. *Phys. Rev. B* **2009**, *79*, 1−7.
(28) Roy, A. K.; Farmer, B. L.; Varshney, V.; Sihn, S.; Lee, J.; Ganguli, S. *ACS Appl. Mater. Interfaces* **2012**, *4*, 545−563.
(29) Shenogin, S.; Xue, L.; Ozisik, R.; Keblinski, P.; Cahill, D. G. *J. Appl. Phys.* **2004**, *95*, 8136−8144.
(30) Gardea, F.; Lagoudas, D. C. *Composites, Part B* **2014**, *56*, 611−620.
(31) Hmina, N.; Scudeller, Y. *Int. J. Heat Mass Transfer* **1998**, *41*, 2781−2798.
(32) Hasselman, D.; Johnson, L. F. *J. Compos. Mater.* **1987**, *21*, 508−515.
(33) Hatta, H.; Taya, M. *J. Appl. Phys.* **1986**, *59*, 1851−1860.
(34) Nan, C.-W.; Birringer, R.; Clarke, D. R.; Gleiter, H. *J. Appl. Phys.* **1997**, *81*, 6692−6699.
(35) Song, Y. S.; Youn, J. R. *Carbon* **2006**, *44*, 710−717.
(36) Tserpes, K. I.; Papanikos, P. *Composites, Part B* **2005**, *36*, 468−477.
(37) Chawla, S.; Naraghi, M.; Davoudi, A. *Nanotechnology* **2013**, *24*, 1−9.
(38) Log, T.; Gustafsson, S. *Fire Mater.* **1995**, *19*, 43−49.
(39) He, Y. *Thermochim. Acta* **2005**, *436*, 122−129.
(40) Swartz, E. T.; Pohl, R. O. *Rev. Mod. Phys.* **1989**, *61*, 605−668.
(41) Parker, W.; Jenkins, R.; Butler, C.; Abbott, G. *J. Appl. Phys.* **1961**, *32*, 1679−1684.
(42) Shenogina, N.; Shenogin, S.; Xue, L.; Keblinski, P. *Appl. Phys. Lett.* **2005**, *87*, 1−3.
(43) Aliev, A. E.; Guthy, C.; Zhang, M.; Fang, S.; Zakhidov, A. A.; Fischer, J. E.; Baughman, R. H. *Carbon* **2007**, *45*, 2880−2888.
(44) Ganguli, S.; Roy, A. K.; Anderson, D. P. *Carbon* **2008**, *46*, 806−817.
(45) Henrici-Olive, G.; Olive, S. The chemistry of carbon fiber formation from polyacrylonitrile. In *Industrial Developments*; Advances in Polymer Science, Vol. *51*; Springer: New York, 1983; pp 1−60.
(46) Momentive. EPON Resin 862 Technical Data Sheet. http://www.momentive.com/Products/TechnicalDataSheet.aspx?id=3950 (December 1, 2012).
(47) Huxtable, S. T.; Cahill, D. G.; Shenogin, S.; Xue, L.; Ozisik, R.; Barone, P.; Usrey, M.; Strano, M. S.; Siddons, G.; Shim, M. *Nat. Mater.* **2003**, *2*, 731−734.

NOTE ADDED AFTER ASAP PUBLICATION

This paper was published on the Web on December 31, 2013, with errors in Figure 8b. The inset images in Figure 8b have been correctly positioned with respect to the graphic, and the corrected version was reposted on December 31, 2013.